Research Square

Preprints are preliminary reports that have not undergone peer review.
They should not be considered conclusive, used to inform clinical practice,
or referenced by the media as validated information.

A Broadband Grating–Split Resonator Transmissive Metasurface for Efficient Terahertz Linear Cross-Polarization Conversion Based on Characteristic Mode Analysis

Harish Raizada[1]

Dr B.R. Ambedkar National institute of Technology ,Jalandhar

Nitesh Kashyap[2]

Kashyapn@nitj.ac.in

Dr B.R. Ambedkar National institute of Technology ,Jalandhar

Research Article

Keywords: Metasurface, Polarization Conversion, Fractional Bandwidth, Polarization Conversion Ratio (PCR), Axial Ratio (A.R)

Posted Date: September 17th, 2026

DOI: https://doi.org/10.21203/rs.3.rs-10682321/v1

License: This work is licensed under a Creative Commons Attribution 4.0 International License.
Read Full License

Additional Declarations: No competing interests reported.

A Broadband Grating–Split Resonator Transmissive Metasurface for Efficient Terahertz Linear Cross-Polarization Conversion Based on Characteristic Mode Analysis

Harish Raizada[1]*, Nitesh Kashyap[2]

[1]Department of Electronics and Communication Engineering, Dr. B. R. Ambedkar National Institute of Technology, Jalandhar 144008, Punjab, India.

[2]Department of Electronics and Communication Engineering, Dr. B. R. Ambedkar National Institute of Technology, Jalandhar 144008, Punjab, India

Abstract

In this paper, we propose a novel three-metal-layer grating-split-resonator transmissive metasurface for broadband linear cross-polarization conversion at terahertz (THz) frequencies. Unlike conventional transmissive polarization converters, the proposed device enables efficient broadband polarization conversion via strong electromagnetic coupling between the polarization-selective metallic gratings and an asymmetric split-ring resonator. The proposed metasurface can not only greatly suppress the co-polarized transmission but also exhibit an almost 100% polarization conversion ratio (PCR > 99%) over a broad frequency range of 0.35–1.45 THz, with a fractional bandwidth (FBW) of 122.2%. A systematic study of the polarization conversion mechanism, using transmission characteristics, surface-current distributions, parametric optimization, and Characteristic Mode Analysis (CMA), demonstrates that Modes 2–4 play a significant role in broadband polarization conversion. The broadband cross-polarization conversion is attributed to the synergistic interaction between the split-ring resonator and the metallic gratings, as further confirmed by comparative studies of the all-grating, all-resonator, and combined configurations. The proposed metasurface can achieve a compact three-metal-layer configuration with a wide operating bandwidth and high polarization conversion efficiency compared with recently published transmissive THz polarization converters. The proposed metasurface has great potential for next-generation THz communications, imaging, sensing, and spectroscopic applications owing to its compact size, effective polarization conversion, and simple multilayer design.

Keywords Metasurface, Polarization Conversion, Fractional Bandwidth, Polarization Conversion Ratio (PCR), Axial Ratio (A.R)

1. Introduction

Metasurfaces were developed by Yu et al. (2013). Since then, they have become an important platform for research on planar optics. In particular, metasurfaces have attracted considerable attention in THz technology owing to their sub-wavelength features and high ability to manipulate electromagnetic waves. Metasurfaces have been employed, for example, for transparency modulation of the EIT effect (Yun et al., 2017), THz vortex beam generation (Feng et al., 2022; Chen et al., 2022), THz polarization conversion, THz abnormal refraction (Xie et al., 2019), THz generation and modulation by ITO-metals (Lu et al., 2021). The amplitude, phase, and polarization state of THz waves can be efficiently controlled by adjusting the geometry of the metasurface unit cell. In other words, the modulation function of the metasurface for THz waves is determined by the architecture of the repeating unit. One of the most studied applications of these functions is polarization conversion, which is of great importance in terahertz communication, imaging, spectroscopy, and sensing systems.

Optical crystals were widely used to control the polarization state of THz waves before the development of metasurfaces. The electro-optic effect would allow the crystal to change the refractive index, thereby altering the polarization state and other wave properties. However, optical crystal photoelectric modulators are bulky and have a limited useful frequency range. Modern metasurface polarization converters can overcome the limitations of optical crystals thanks to their compact structure, high bandwidth, and stable incident-angle tolerance. One example is the linear polarization converter reported by Xu et al. (Jing et al., 2018). The design offers better polarization conversion performance while adhering to the Fabry-Pérot resonance principle. For THz polarization conversion, a variety of metasurface geometries have been reported, such as nanoscale metal rods (Zhao & Alu, 2013), circular split ring resonators (Yang et al., 2020), single ring and vanadium dioxide composite structures (Yan et al., 2022) (Feng et al., 2022), or metal oscillating rods with an arrow shape (Jiang et al., 2021). These anisotropic metasurface configurations have exhibited polarization conversion by modulating the electromagnetic response. Nevertheless, progress towards simpler, broadband-transmissive polarization converters is constrained by structural complexity and fabrication requirements.

To overcome these limitations, a variety of metasurface-based polarization converters have been proposed in recent years. For example, the circular polarization converter proposed by Jia M et al. (Jia et al., 2019) can cause the left- and right-handed optical rotations to deviate in opposite directions over the frequency range 0.3–0.9 THz, depending on the abnormal transmission mode. The rotation angle of each element should be designed to achieve circular-polarization wave separation, which is also challenging in a metal-structure polarization converter. Nevertheless, the suggested circular polarization converter is difficult to fabricate and has a complicated design. Zhou et al. developed a metasurface polarization converter (Zhou & Li, 2020) for linear-to-x-y polarization conversion in the 1.0–2.0 THz range. However, this structure's metasurface requires precise connections between various shapes, making wide-scale application challenging. A tapered metasurface polarization converter that achieves polarization conversion over 0.6–1.4 THz was developed by Xu et al. However, this structure can only be created as a reflection-type structure because it uses the F-P resonator principle. An ultra-wideband, transmissive Terahertz Linear Cross Polarization Converter with high polarization conversion efficiency, operating between 4.442 THz and 8.444 THz, was presented by [Sheheryar et al., 2025]. The design, however, is inclined toward multifunctionality, offering space for a smaller, physically simple transmissive polarization converter for broadband THz applications. A broadband, asymmetric, transmissive THz co-to-cross-polarization converter was developed by [Khalichi et al.,2025]. Nevertheless, unlike a simple broadband linear-polarization converter, this paper focused more on asymmetric transmission. A transmissive THz linear polarization converter based on anisotropic metamaterials has been proposed by [Zhao et al. 2025]. Even with such advances in research, it remains extremely challenging to achieve ultra-broadband polarization conversion with a simple design and high efficiency. However, designing an ultra-small, transmissive THz polarization converter with both ultra-broad bandwidth and high polarization conversion efficiency remains a challenging problem despite the above-mentioned breakthroughs.

Motivated by these challenges, a broadband transmissive polarization converter based on a double-layer metasurface is proposed. In this work, a broadband transmissive polarization converter based on a double-layer metasurface is proposed. A broadband polarization conversion response from approximately 0.35 THz to 1.45 THz has been numerically demonstrated; the absolute bandwidth is 1.25 THz, and an exceptionally wide fractional bandwidth of 122.2% has also been reported. Moreover, over almost the entire operating frequency range, the polarization conversion efficiency approaches unity. This broadband performance is achieved through the synergistic excitation and coupling of multiple resonant modes via the double-layered metasurface, thereby significantly extending the operating bandwidth without sacrificing conversion efficiency. The suggested design is appropriate for broadband terahertz polarization modification in sensing, spectroscopy, communication, and imaging applications due to its features.

The key contribution of my proposed work is:

- Design of a compact double-layer transmissive THz metasurface employing orthogonal metallic gratings and a butterfly-wing resonator.
- Achievement of 0.35–1.45 THz broadband polarization conversion with a 122.2% fractional bandwidth.
- Realization of near-unity PCR across almost the entire operating frequency range.
- Demonstration that multiple resonant modes dominate the broadband polarization conversion mechanism through CMA and field analyses.
- Implementation of a fabrication-compatible structure suitable for standard terahertz microfabrication processes.

2. Basic Concept

Polarization provides the best description of the spatial properties of electromagnetic wave propagation. The electric field vectors of the incident and transmitted electromagnetic waves can be depicted as follows when an X-polarized electromagnetic wave is incident on a terahertz polarizer metasurface [23-25].

$$\widehat{\mathrm{E}}_{\mathrm{i}} = \mathrm{E}_{\mathrm{y}}^{\mathrm{i}} \mathrm{e}^{-\mathrm{jkz}} \hat{\mathrm{y}}_{\mathrm{o}} + \mathrm{E}_{\mathrm{x}}^{\mathrm{i}} \mathrm{e}^{-\mathrm{jkz}} \hat{\mathrm{x}}_{\mathrm{o}}, \quad (1)$$

$$\widehat{\mathrm{E}}_{\mathrm{t}} = \mathrm{E}_{\mathrm{y}}^{\mathrm{t}} \mathrm{e}^{-\mathrm{jkz}} \hat{\mathrm{y}}_{\mathrm{o}}^{\mathrm{t}} + \mathrm{E}_{\mathrm{x}}^{\mathrm{t}} \mathrm{e}^{-\mathrm{jkz}} \hat{\mathrm{x}}_{\mathrm{o}}^{\mathrm{t}}, \quad (2)$$

Where E_{ix} and E_{iy} indicate the components of the incident electromagnetic waves in the X direction and the Y direction, respectively. E_{tx} and E_{ty} indicate the components of the electromagnetic waves that are transmitted in the X- and the Y direction, respectively. "x_o" and "y_o" are unit vectors along the X axis and the Y axis, respectively. The theory of polarization conversion is illustrated in Fig.1.

Equation (2) can be expressed as follows: define the cross-polarization transmission coefficient $t_{yx} = |E_y^t|/|E_x^i|$ and the co-polarization transmission coefficient $t_{xx} = |E_x^t|/|E_x^i|$

$$\hat{E}_t = t_{yx} E_x^i e^{-jkz} \hat{y}_o^t + t_{xx} E_x^i e^{-jkz} \hat{x}_o^t , \quad (3)$$

$$\hat{E}_t = t_{yx} E_x^i e^{-j(kz-\phi_{yx})} \hat{y}_o^t + t_{xx} E_x^i e^{-j(kz-\phi_{xx})} \hat{x}_o^t , \quad (4)$$

The transmission phase from X-polarization to Y-polarization is ϕ_{xy}, whereas the transmission phase from X-polarization to X-polarization is ϕ_{xx} The electric field component in the Y-direction with the equation $\hat{E}_t = t_{yx} E_x^i e^{-j(kz-\phi_{yx})} \hat{y}_o^t$ is the Y-polarization wave for xx = 0 as per equation (3).

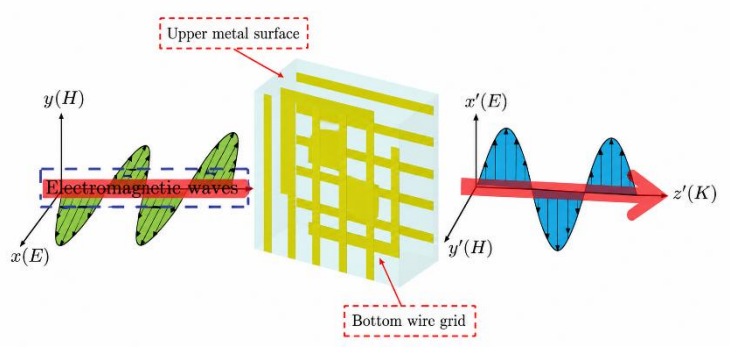


Fig.1. Terahertz polarization converter layout diagram.

The PCR is used to determine the polarization converter's conversion efficiency [26, 27].

$$PCR = \frac{t_{yx}^2}{t_{yx}^2 + t_{xx}^2} \tag{5}$$

Transmittance (dB) is defined as follows in order to describe the performance of the planned polarization converter:

$$T_{yx} = 10\log_{10}\left(\frac{I_y^t}{I_x^i}\right) = 20\log_{10}\left(\frac{E_y^t}{E_i^x}\right) = 20\log_{10}t_{yx} \tag{6}$$

The polarization state of the electromagnetic wave changes from the polarization state in the x to y direction to the polarization state, denoted by the x subscript. The Stokes parameter technique is used in this paper to represent the transmitted wave, as described in [28,29].

$$\begin{pmatrix} S_0 \\ S_1 \\ S_2 \\ S_3 \end{pmatrix} = \begin{pmatrix} t_{xx}^2 + t_{yx}^2 \\ t_{xx}^2 - t_{yx}^2 \\ 2t_{xx}t_{yx}cos\delta \\ 2t_{xx}t_{yx}sin\delta \end{pmatrix} = \begin{pmatrix} I_{xx} + I_{yx} \\ I_{xx} - I_{yx} \\ I_{\pi/4} - I_{-\pi/4} \\ I_R - I_L \end{pmatrix} \tag{7}$$

where I_R and I_L represent the intensity of right and left circularly polarized light, respectively; $I_{\pi/4}$ represents the intensity of the linearly polarized light component of the π/4 light-wave direction; and $I_{-\pi/4}$ represents the intensity of the linearly polarized light component of the -π/4 light-wave direction. The polarization rotation angle (PRA) ψ, and the ellipticity angle (EA)χ [30] can be defined as follows to explain the linear polarization characteristics of polarized electromagnetic waves.

$$tan2\psi = \frac{S_2}{S_1} \tag{8}$$

$$sin2\chi = \frac{S_3}{S_0} \tag{9}$$

and

$$\psi = \frac{1}{2}arctan\left(\frac{2t_{xx}t_{yx}cos\delta}{t_{xx}^2 - t_{yx}^2}\right) \tag{10}$$

$$\chi = \frac{1}{2}arcsin\left(\frac{2t_{xx}t_{yx}sin\delta}{t_{xx}^2 + t_{yx}^2}\right) \tag{11}$$

According to the theory of electromagnetic waves, it is found that whenever the current distribution between the layers of multilayered metamaterials or within a single layer of metamaterial is induced by the incidence of electromagnetic waves such that it forms a small current loop, then at this point, the small current loop may be considered equivalent to a magnetic dipole, which induces magnetic resonance and thus generates a magnetic moment. When the distribution of surface current of the metasurface device is similar to a current stub, then the current stub may be said to be similar to an electric dipole, where electric resonance occurs. The dipole moment of the electric dipole is responsible for the modulation of the electromagnetic wave [31-33]. Therefore, when an electromagnetic wave interacts with the metallic metasurface, it undergoes electromagnetic resonance at different frequencies. The magnetic or electric dipole moment thus modulates the incident electromagnetic wave, causing its polarization [34-36].

3. Unit Cell Configuration and Fabrication Process

Fig. 2 shows the geometry of the proposed transmissive linear polarization converter. Fig. 2(a) shows the 3D perspective view of the unit cell, Figure 2(b) shows the intermediate butterfly-wing

resonator, and Fig. 2(c) shows the orthogonal grating layers. The unit cell consists of three metal layers separated by two dielectric substrates. The top and bottom metallic layers are metallic gratings with orthogonal orientations, while the intermediate metallic layer is a modified butterfly-wing resonator with two symmetrical incisions in the circular metallic patch. The multilayer structure is the basis for broadband polarization conversion. It introduces structural anisotropy and enables effective interaction between the incident electromagnetic wave and the resonant metallic elements. The metallic layers are supported by two F4B dielectric substrates with a thickness of 30 μm, a relative permittivity $\varepsilon r = 3.0$, and a loss tangent $\tan \delta = 0.002$. Low dielectric loss in the substrate decreases propagation loss while maintaining electromagnetic contact between neighboring metallic layers. All metallic patterns are copper with a uniform thickness of 0.3 μm and an electrical conductivity of 5.8 × 107 S/m, so that the ohmic loss is low in the operating frequency range. The top metallic layer comprises periodically spaced vertical strips, and the bottom layer has the same strips oriented horizontally, creating an orthogonal grating structure. Here, $W_2 = 5$ μm and $d = 20$ μm are the strip width and spacing, respectively. The butterfly-wing resonator, embedded between the two grating layers, exhibits multiple resonant modes due to interactions between the orthogonal metallic patterns.

This resonant behavior allows efficient polarization conversion and improves the impedance matching over a broad frequency range. The optimum geometrical parameters of the unit cell are $Px = Py = 100$ μm, $L_1 = 68$ μm, $W_1 = 9$ μm, and the outer radius of the resonator $R = 25$ μm. The dimensions were estimated by parametric optimization and systematic full-wave electromagnetic simulations. Changes in these parameters altered transmission and impedance-matching properties, as well as resonant frequencies, resulting in significant changes in the operating bandwidth and polarization conversion performance. The optimum dimensions are chosen to achieve broadband operation and high polarization conversion efficiency. The proposed multilayered transmissive metasurface can be realized through existing microfabrication techniques. Photolithography is initially employed to pattern both the metallic gratings and the butterfly-wing resonators on the F4B substrates. Deposition of copper, followed by lift-off, is subsequently employed to pattern the metallic structures. All layers that make up the complete multilayered structure are bonded together through precise alignment. The proposed design is suitable for existing fabrication processes, as these techniques have been successfully applied to THz metasurfaces.

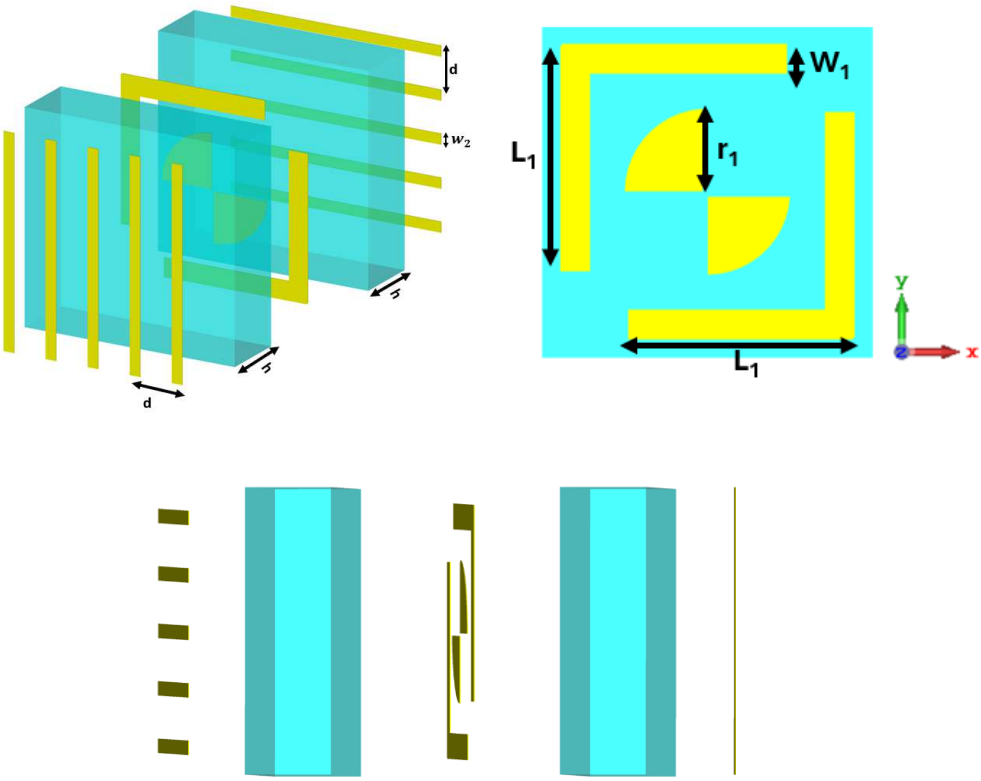


Fig.2.Diagrammatic representation of the transmission unit: (a) perspective view; (b) intermediate subsurface view; (c) left view

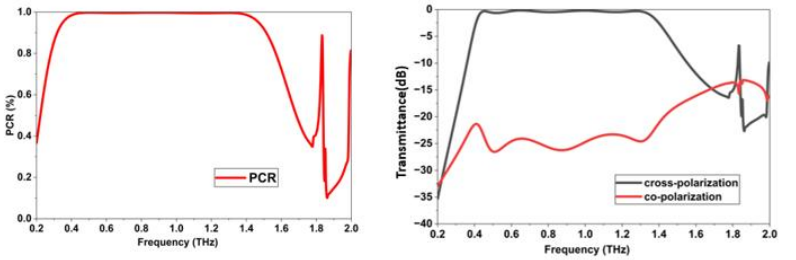
Each of the three metallic layers constituting the proposed transmissive metasurface plays a distinct electromagnetic role. First of all, surface currents are induced by the incident linearly polarized wave at the receiving interface that constitutes the top metallic grating layer. This grating layer couples the energy of the incoming wave to the intermediate resonant layer due to its anisotropic geometry. The principal resonance element of the unit cell is the central butterfly-wing resonator. It can support strong localized surface currents that excite both electric and magnetic resonances, owing to its modified geometry comprising symmetrical slots and metal arms. Because it emits this energy orthogonally polarized and linearly in the direction of the output face, the lower orthogonal metallic grating acts as the transmitting interface. Consequently, many resonant modes are generated by the interaction among the transmitting grating, resonant element, and receiving grating, resulting in broadband polarization conversion with high transmission efficiency.

4. Results and Discussion

The primary performance metric used to assess the polarization conversion performance of the suggested transmissive metasurface is the polarization conversion ratio (PCR), which is defined as

$$PCR = \frac{T_{CRO}^2}{T_{CRO}^2 + T_{COO}^2} \tag{12}$$

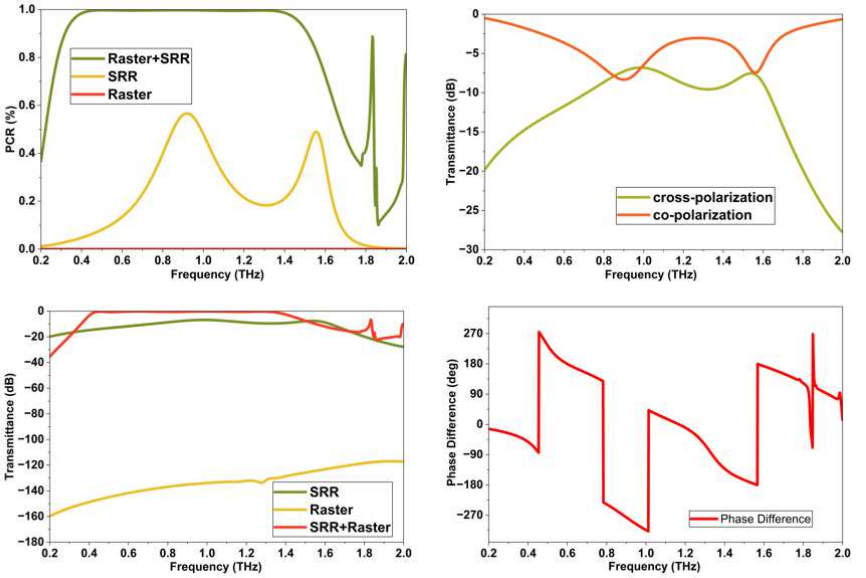
where T_{CRO} and T_{COO} are the magnitude cross-polarized and co-polarized transmission coefficients, respectively. When the value of PCR is close to 1, the incident linearly polarized wave is almost completely converted to the orthogonal polarization state after passing through the metasurface. The performance of the proposed transmissive metasurface for polarization conversion is illustrated in Fig. 3(a) and 3(b), calculated using Equation (12). The PCR is plotted in Fig. 3(a), while Fig. 3(b) shows the transmission coefficients of the cross-polarization (Txy) and co-polarization (Tyy) components. It is obvious that an efficient linear polarization conversion occurs in the considered metasurface over a broad frequency range. The PCR shows high polarization conversion, with PCR 1 spanning 0.35-1.45 THz. It should be noted that the presence of resonant modes within the butterfly wing resonator leads to an increase in the PCR value. This phenomenon occurs due to the gradual increase of cross-polarized transmission and coupling between the orthogonal metallic gratings. Impedance matching significantly reduces co-polarized transmission at resonant frequencies, resulting in unity PCR. Moreover, the polarization conversion process is confirmed by the transmission properties shown in Fig. 3(b). The cross-polarization transmission coefficient is significantly higher than the co-polarization transmission coefficient over the operating bandwidth. The co-polarization transmission is attenuated to less than −20 dB, thereby creating polarization isolation of more than



(a) **(b)**

Fig. 3. Simulation of the proposed transmissive metasurface: (a) PCR, and (b) Co- and cross-polarized transmission coefficients.

0.35 to 1.45 THz. 20 dB over a wide bandwidth, whereas cross-polarization transmission remains around 0 dB over most of the operating frequency range. The power transmission is mainly



converted to orthogonal polarization.

Fig. 4. Simulation of the proposed transmissive metasurface: (a) PCR of different structural configurations, (b) co- and cross-polarized transmission coefficients, (c) transmission responses of the raster-only, SRR-only, and combined metasurface, and (d) phase difference between the transmitted polarization components.

To determine the role of each metallic structure in polarization conversion, the polarization conversion characteristics of the entire metasurface, only the SRR structure, and only the Raster structure have been analyzed. The entire metasurface exhibits the highest polarization conversion efficiency among the cases, as shown in Fig. 4(a). In the 0.35–1.45 THz operating range, the PCR value remains unity and rapidly increases from 0.36 at 0.2 THz to more than 0.99 at 0.35 THz. Such a wide-range operation can be attributed to the cooperative action of the orthogonal metallic structures and the butterfly-wing resonator, which has multiple resonance states and enhances the coupling between the incident wave and the cross-polarized transmitted wave. Higher co-polarized transmission, along with lower cross-polarized transmission, is achieved because the resonant coupling becomes weaker as the frequency increases above 1.45 THz. Hence, numerous resonance oscillations can be observed in the 1.80-2.00 THz frequency range as the PCR decreases. On the other hand, owing to the absence of orthogonal grating layers, the electromagnetic coupling required to achieve polarization rotation is significantly reduced, resulting in inadequate polarization conversion capability. Therefore, the maximum PCR is 0.56 at 0.90 THz and 0.48 at 1.55 THz. The grating layer alone cannot provide an efficient mechanism of cross-polarized transmission, as indicated by the almost negligible PCR achieved from the raster-only layer across the entire frequency band. Instead, it does not facilitate the resonant polarization conversion process but serves as a frequency-selective transmission layer. The results confirm that broadband polarization conversion with high efficiency can be achieved only by combining the two structures. The physical explanation of the broadband polarization conversion mechanism is provided by comparing the structures of the raster-only, SRR-only, and the proposed combined structures. In the case of raster-only, the absence of a localized resonance structure makes it behave primarily as an anisotropic coupling medium and permits only weakly scattered resonances. Thus, the polarization conversion occurs partially. In turn, the localized resonances resulting from surface currents circulating along the split-ring structure are observed in the SRR-only structure. However, these resonances provide narrowband polarization conversion because of their pronounced frequency selectivity. Electromagnetic coupling of a strong nature occurs between the raster and SRR when the two elements are integrated together into one unit cell. Although many resonant modes are generated by the SRR, the raster helps couple the incoming electromagnetic wave to the SRR. As a result, resonance hybridization occurs, reducing the frequency separation between adjacent resonant modes. Therefore, continuous broadband polarization response is obtained due to resonance overlap. Broadband response cannot be obtained from either component individually; however, when they act together, ultra-broadband polarization conversion can be achieved.

As shown in Fig. 4(b), the transmission characteristics of the overall metasurface have been demonstrated. Within the operational bandwidth of 0.35 to 1.45 THz, the cross-polarization transmission is significantly larger than the co-polarization transmission. In the same frequency band, the co-polarization transmission varies from -8 dB to -3 dB, whereas the cross-polarization transmission varies from -10 dB to -7 dB. Most of the energy transmitted is converted to an orthogonal polarization state, as observed in the transmission behavior. Above 1.5 THz, the PCR deteriorates due to increased co-polarization and decreased cross-polarization transmission. To determine the performance of the Raster-only, SRR-only, and Raster + SRR configurations in terms of transmission, Fig. 4(c) illustrates the results. Since the input wave is completely hindered by the metal grating, the transmission of the raster-only configuration is very low (below -120 dB). While providing some transmission, the SRR-only configuration fails in converting the polarization.

The interaction between the two metallic layers not only increases transmission but also the efficiency of polarization conversion, as illustrated by the high transmission of the full Raster + SRR configuration. Fig. 4(d) depicts the phase difference between the transmission coefficient of the co-polarization state and the transmission coefficient of the cross-polarization state. The phase

difference shows several phase jumps due to resonance-phase wrapping. The presence of anisotropic electromagnetic behavior and the efficient phase control by the proposed metasurface are evident from the ±270° phase difference. The polarization rotation angle is presented in Fig. 4(d). The smooth variation in the polarization rotation angle, with values close to 0°, indicates a stable linear-polarization conversion process with negligible distortion of the polarization state. The faster changes in the polarization rotation angle above 1.65 THz are due to higher-order resonances and correspond to the drop in the PCR shown in Fig. 3(a). Based on the PCR results, the transmission, phase response, and polarization rotation angle properties indicate that the proposed Raster + SRR metasurface is an efficient broadband linear polarization converter. In addition to the polarization conversion ratio (PCR), the total transmission efficiency and insertion loss were analyzed to evaluate the effectiveness of the proposed transmissive polarization converter.

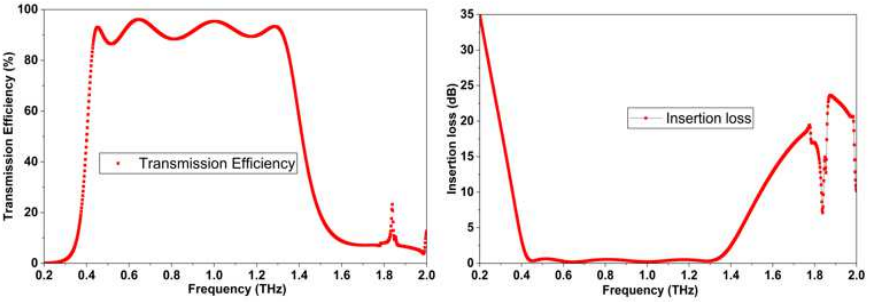


Fig. 5. Transmission performance of the proposed transmissive polarization converter (a) Total transmission efficiency, (b) Insertion loss analysis

Even though the good polarization conversion can be defined by a high PCR, high transmission efficiency cannot be assumed. Hence, the power transmission through both cross-polarized and co-polarized rays was considered. As shown in Fig. 5(a), the proposed metasurface achieves more than 90% transmission efficiency over the operating frequency band from 0.35 to 1.45 THz. This means that effective transmission of electromagnetic energy, rather than simultaneous suppression of both transmitted polarizations, leads to high PCR. Furthermore, as shown in Fig. 5(b), the proposed metasurface exhibits an insertion loss of approximately 1 dB or less over the frequency band 0.35-1.45 THz; hence, almost all of the incident power is transferred. Thus, the proposed metasurface provides broadband polarization conversion with very good transmission properties and can be used for practical terahertz communication and imaging applications. The limited conductivity of the metallic resonator not only affects the resonance characteristics but also the electromagnetic response at terahertz frequencies. In the present design, copper with a conductivity of 5.8×107 S/m was used. At THz frequencies, the skin depth reduces to the nanoscale, confining the induced current to a thin surface layer and leading to finite ohmic losses. Therefore, conductor losses increase with frequency and may somewhat reduce the transmission efficiency, especially in the higher end of the operational range. Nonetheless, the suggested metasurface's metal thickness is significantly greater than the equivalent skin depth, guaranteeing effective current confinement and reducing resistive losses across the operating band. Therefore, higher-order resonant mode excitation, increased phase mismatch under oblique incidence, and the steady rise in conductor losses associated with finite conductivity are the main causes of the observed degradation beyond about 1.5 THz. The metallic resonator has a thickness of $0.3\mu m$ (300nm), while the skin depth of copper at the highest operating frequency(2THz) is approximately 47nm, calculated by using equation (13)

$$\delta = \sqrt{\frac{2}{\omega \mu_o \sigma}} \tag{13}$$

Thus, the induced current is well confined to the conductor surface when the metal thickness is

more than six times the equivalent skin depth. Consequently, the effect of insufficient metal thickness on the effective conductivity is negligible, and the additional conductor losses are negligible over the operating band. At terahertz frequencies, the finite conductivity leads to unavoidable ohmic losses that have little effect on transmission efficiency. The slight performance deterioration near the top of the operating range is mainly due to the excitation of higher-order resonant modes and an increase in phase mismatch, rather than to insufficient metal thickness.

5. Surface Current Distribution

To understand the physical mechanism of the proposed transmissive metasurface, we investigate the surface current distributions at four sample resonance frequencies, 0.42 THz, 1.00 THz, 1.28 THz, and 1.84 THz, as shown in Fig. 6. The outer C-shaped resonator and the metallic grating strips receive most of the induced current at 0.42 THz. The current flows mostly along the vertical parts of the resonator and weakly along the inner semicircular patches. The reverse flow directions between the front and back metallic gratings indicate the formation of a magnetic resonance. The unit cell works in its fundamental resonant mode and provides the first electromagnetic coupling required for polarization conversion at this frequency. In the case of frequency 1.00 THz, there is a significant rise in the magnitude of current along with its distribution through the outer as well as the semi-circular inner resonators. Current accumulation can be observed at the bends of the C-shaped resonator, suggesting increased capacitive coupling. In this case, the excitation of multiple metallic parts enhances electric and magnetic resonances and their coupling. At 1.28 THz, the surface current is more evenly distributed over the resonator than at lower-frequency resonance, and some current paths change direction. Strong current localization is observed in the horizontal connecting sections and the inner resonators, suggesting the excitation of a higher-order resonant mode. The presence of multiple resonant current loops significantly enhances polarization conversion by effectively suppressing the co-polarized transmitted component and boosting the cross-polarized transmitted field.

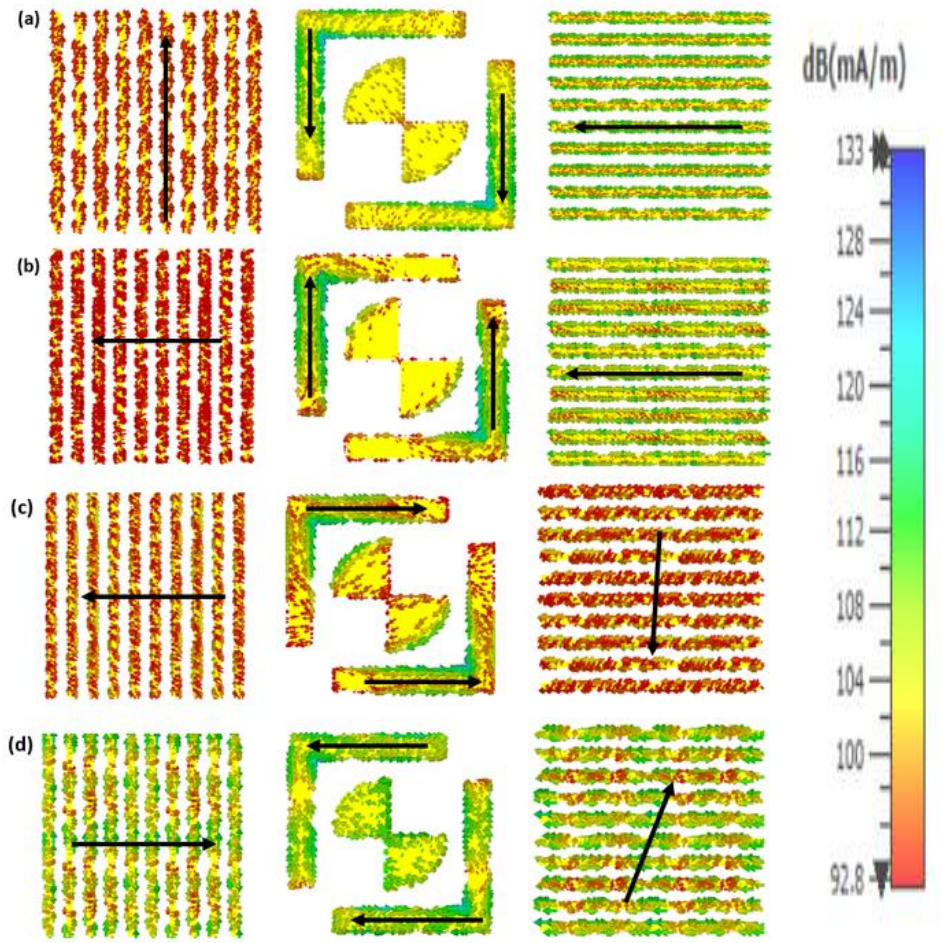


Fig.6. SCD (a) 0.42 THz, (b) 1 THz, (c) 1.28 THz, and (d) 1.84 THz

The induced current at 1.84 THz is present throughout the entire metallic structure, including the gratings, the outer resonator, and the inner resonating elements. The complicated distribution of current loops suggests strong higher-order resonances and enhanced near-field coupling between top and bottom metallic layers. These multiple resonances work together to keep effective transmission characteristics at higher frequencies and extend the working bandwidth. The surface current distributions show that the polarization conversion mechanism varies slowly with frequency. At 0.42 THz, most of the induced current is on the metallic grating strips and outer C-shaped resonator. The excitation of the initial magnetic resonance that induces polarization conversion is evidenced by the opposite directions of the currents in the front and rear gratings. The current spreading across the inner and outer parts of the resonator as the frequency increases to 1.00 THz is also observed, attributed to enhanced capacitive coupling between the resonator and the orthogonal metallic gratings due to current accumulation around the split regions. This enhanced electromagnetic interaction not only enhances the resonant response but also improves the polarization conversion performance. At 1.28 THz, higher-order resonant behavior is excited, in which the current is more evenly distributed across the resonator, and new current paths form along the horizontal connecting sections. Such resonance responses can provide effective polarization conversion across the entire operational frequency range and enhance electromagnetic interaction within the three-layer structure. At 1.84 THz, the current spreads over the whole metallic structure,

suggesting higher-order resonances outside the main working band. The electromagnetic coupling between the orthogonal metallic gratings and the modified split resonator gradually increases as successive resonant modes are excited at higher frequencies, resulting in broadband polarization conversion over the 0.35–1.45 THz range. The Characteristic Mode Analysis also supports this interpretation since the dominant Modes 2-4 correspond to the principal resonant behavior observed within the operating band.

Table 1. Physical Interpretation of the Polarization Conversion Mechanism

Frequency	Resonance Type	Physical Role
0.42 THz	Fundamental electric–magnetic resonance	Starts broadband conversion
1.00 THz	Hybrid coupled resonance	Strengthens coupling
1.28 THz	Higher-order resonance	Extends the upper operating band
1.84 THz	Higher-order mode	Outside operating band

The 90^0-polarization rotation is achieved by simultaneously exciting electric and magnetic resonances in the proposed three-layer metasurface. The induced currents are concentrated at the discontinuities of the modified C-shaped resonator, giving rise to the electric dipole resonance, and the anti-parallel current distributions between the front and back metallic gratings induce the magnetic dipole resonance. The orthogonal resonant responses interact to modify the transmitted electromagnetic field, converting the incident linear polarization to its orthogonal polarization. When the operating frequency is increased from 0.42 THz to 1.28 THz, the current loops are stronger and spread over a larger area of the resonator, which shows improved electromagnetic coupling between the metallic gratings and the resonator. This is achieved by simultaneously exciting electric and magnetic dipole resonances, thereby enabling effective polarization conversion over the broadband operating range. The current distribution at 1.84 THz is mostly indicative of higher-order resonant behavior outside the main working band.

6. Parametric Analysis

To achieve optimal transmission and polarization conversion, a systematic parametric study was conducted to vary the key geometrical parameters of the proposed unit cell. All other structural parameters were fixed at the ideal values during each parametric sweep. The influence of the unit-cell periodicity on the polarization conversion performance was studied by varying the periodicity (P) from $70\mu m$ to $120\mu m$ while maintaining all other geometrical parameters constant. The corresponding PCR reactions are shown in Fig. 7. The electromagnetic coupling between nearest-neighbor unit cells and the phase accumulation across the metasurface are greatly modified by increasing the periodicity, leading to changes in the resonance characteristics and polarization conversion performance. For P=70 μm, the proposed metasurface exhibits relatively poor polarization conversion, particularly in the low-frequency range (0.6-1.1 THz), where strong coupling between neighboring unit cells leads to a significant reduction in PCR. The reduced periodicity modifies the effective surface impedance and reduces excitation of the desirable resonant modes. With the periodicity increased to P=90um, the PCR is significantly enhanced over a wider frequency range, which can be attributed to improved impedance matching and stronger stimulation of the anisotropic resonant modes. The polarization conversion performance reaches a maximum at P = 100 μm. At this periodicity, the proposed metasurface exhibits efficient cross-polarization conversion and good transmission properties, with a PCR close to 1 across the broadest operating bandwidth. The improvement is due to an optimal balance between phase compensation and near-field coupling, which effectively excites multiple resonant modes and suppresses undesired scattering losses. However, the PCR gradually deteriorates as periodicity increases, reaching P=120 μm at frequencies above approximately 1.5 THz. The resonance shift, poor impedance matching, and lower polarization conversion efficiency are due to the larger unit-cell spacing, which reduces near-field interaction between adjacent resonators. Consequently, the high-

frequency region is affected more, and the operational bandwidth is reduced

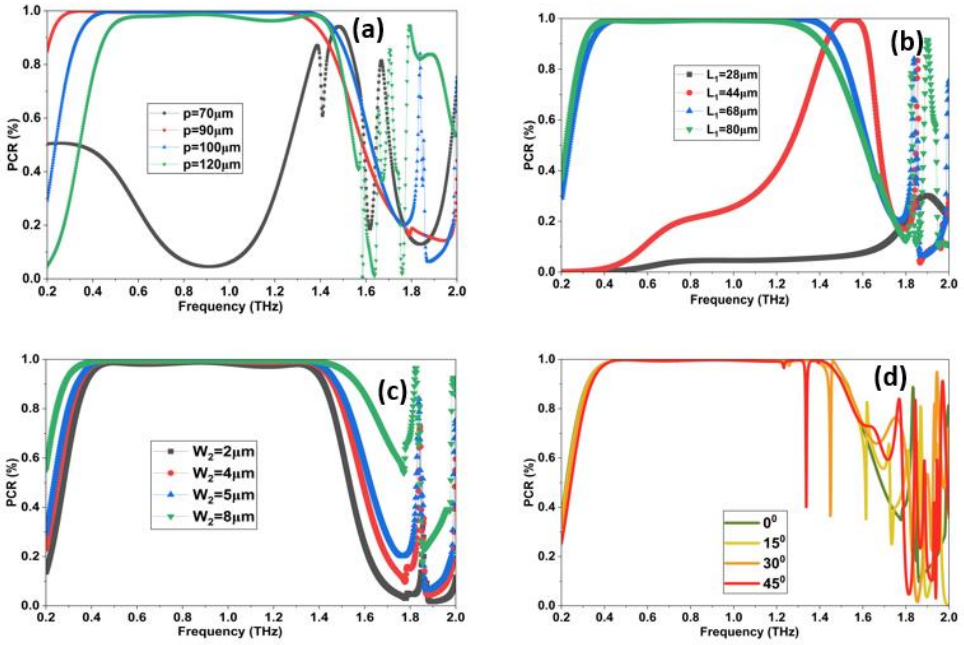


Fig.7. Parametric analysis of the suggested transmissive metasurface: (a) how the polarization conversion ratio (PCR) is affected by periodicity (P), (b) side-arm length (L_1), and (c) grating width (W_2),(d) oblique incidence angle

Hence, P=100μm was selected as the optimal periodicity for the proposed transmissive metasurface, as it exhibits the most stable transmission response, the largest effective operating bandwidth, and the best polarization conversion ratio among all the samples studied. The effect of side-arm length (L_1) on the polarization conversion ratio (PCR) was studied by increasing L_1 from 28 μm to 80 μm, while maintaining the same geometrical parameters shown in Fig. 7(b). The results show that L_1 significantly affects electromagnetic coupling and the unit cell's resonant behavior. For L_1=28 μm, the PCR is relatively low over most of the operational band, indicating insufficient coupling. The side-arm length is increased to enhance coupling strength and significantly improve polarization conversion performance. Optimal results are observed with L_1 = 68μm, demonstrating efficient broadband polarization conversion, with the PCR remaining nearly unity over the widest frequency band. Higher L_1 values (80μm) at high frequencies slightly degrade the PCR value and alter the resonance modes. Consequently, L_1 = 68 μm was determined to be the optimal side-arm length for the proposed metasurface. In Fig. 7(c), the effect of the grating width (W_2) on PCR is investigated by varying W2 from 2 μm to 8 μm, while keeping the other geometric parameters constant. The electromagnetic coupling and impedance matching in the proposed metasurface depend highly on the grating width. PCR decreases as frequency increases for W_2 = 2 μm due to weak coupling between the resonator and the metallic grating. An increase in width widens the PCR operating range. For W_2=5μm, the cross-polarization conversion is effective, and PCR remains one of the widest frequency regions. However, increasing the grating width to W2=8 μm results in performance degradation at high frequencies and alters the resonant modes. The optimal grating width for the proposed metasurface is W_2 = 5μm. The PCR of the proposed transmissive metasurface at incidence angles of 0°, 15°, 30°, and 45° is shown in Fig. 7(d). Within the frequency range from approximately 0.35 to 1.45 THz, the metasurface demonstrates good angular stability and maintains high PCR performance (PCR = 100%). This is due to variations in the tangential wave vector and to an enhanced phase shift across the dielectric layer at higher incidence angles,

leading to a small resonance shift. The lack of any noticeable change in the lower-frequency resonances suggests that the incidence angle affects them minimally. On the other hand, the higher-order resonant state is more sensitive to oblique incidences beyond about 1.5 THz because of the strong influence of phase-matching and symmetry of the electric field distribution. The PCR drops at higher frequencies because cross-polarized transmission decreases with increasing phase mismatch as the incident angle approaches 30° or 45°. Nevertheless, across a wide range of incident angles, the proposed metasurface achieves high polarization conversion efficiency, making it applicable to real-world THz polarization control applications.

7. Characteristic Mode Analysis

To investigate the polarization conversion mechanism of the proposed metasurface, a Characteristic Mode Analysis is performed. The characteristic modes are a set of orthogonal current distributions that are independent of the external excitation. The CMA formulation is given by the following weighted eigenvalue equation (13) [F. H. Lin and Z. N. Chen et al., 2017]:

$$XJ_n = \lambda_n R J_n \tag{13}$$

Where J_n and λ_n represent the characteristic current and eigenvalue of the nth mode, respectively [X. Gao *et al.*,2021]. A characteristic mode is considered strongly radiating when its modal significance, MS, approaches unity, and is defined as a

$$MS = \left|\frac{1}{1+\lambda_n}\right| \tag{14}$$

As shown in Fig. 8, Mode 2 exhibits significant modal excitation in the frequency range from 0.95 to 1.28 THz, with modal significance close to 1. Mode 4 has modal significance close to one in the frequency range between 0.92 and 1.48 THz, whereas Mode 3 has resonance in the range of 0.88-1.22 THz. The presence of broadband polarization conversion is partly due to the overlap of excitation among the above modes, leading to numerous resonances. Thus, they are selected as the dominant modes responsible for the metasurface's electromagnetic response. On the other hand, Modes M1 and M5 have relatively low modal significance across the entire frequency range and are therefore neglected in the subsequent analysis.

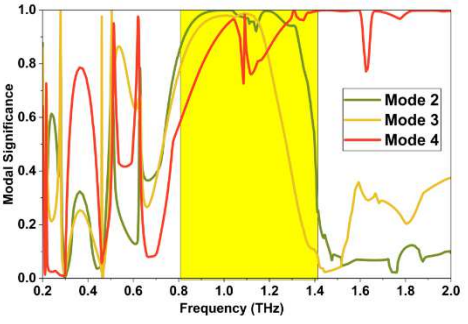


Fig. 8. Modal Significance

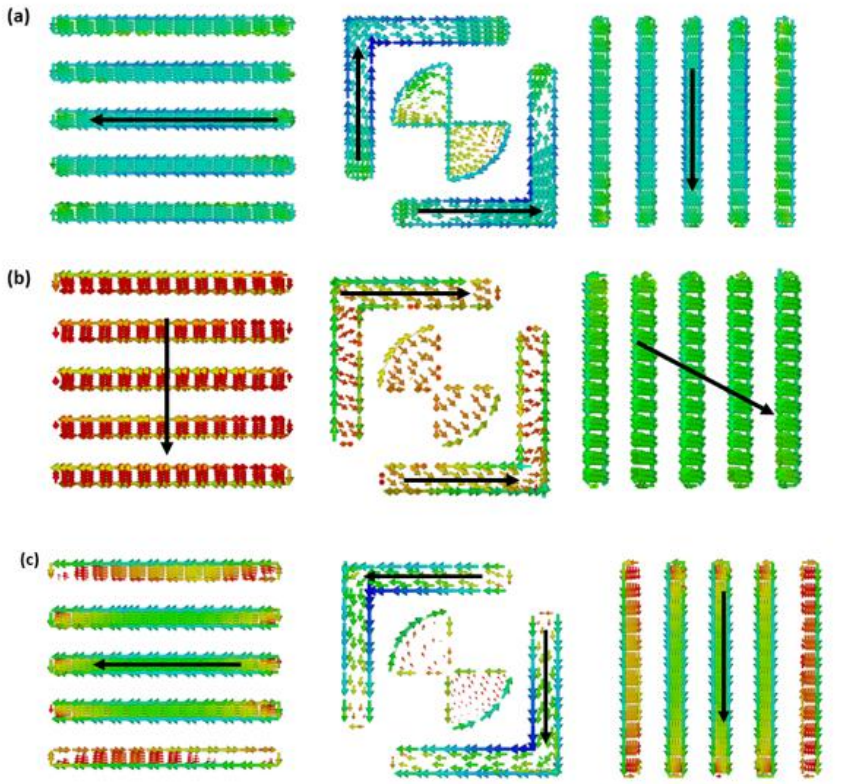


Fig. 9. Modal surface current distributions of the dominant modes: (a) Mode-2 at 1.1THz and (b) Mode-3 at 1THz, (c) Mode-4 at 1. 3THz, denoting linear polarization

Surface currents are largely confined to the horizontal strips of the grating and the outer square-shaped resonator at 1.10 THz. Activation of the fundamental resonant mode is indicated by a uniform current distribution across the metallic structures, with a pronounced current concentration at the strip edges. High cross-polarized radiation occurs within the operational bandwidth due to the effective coupling of the incident wave to its orthogonal components via the current distribution. In Mode 3, the longitudinal current flow is enhanced by the grating strips, while the surface current is spread across the split-ring resonator and the circular segments. The polarization-conversion bandwidth is further increased by resonator-grating coupling, thereby creating a new resonant path. The current distribution in the present case is much more uniform on the grating strips and the resonator at 1.30 THz, with some current density near the metallic boundaries. At the high end of the operational frequency band, this higher-order resonance ensures good cross-polarized transmission and enhances impedance matching. The broadband polarization conversion capability of the proposed metasurface results from the excitation of Modes 2 to 4 simultaneously. The resonance path for Mode 2 (1.10 THz) is realized by limiting the current distribution to the grating stripes and the resonator structure. Orthogonal current distribution is stimulated in order to facilitate cross-polarization transition due to the current redistribution in the center resonator for Mode 3 (1.00 THz). The current distribution is even for the Mode 4 (1.30 THz) resonance path, enabling broadband cross-polarization transmission.

Table1. Recent THz Transmissive Polarization Converters: A Comparison of Their Performance

Ref	Structure	Periodicity	Substrate thickness	No of Metallic Layer	Fabrication complexity	Operating Frequency (THz)	FBW (%)	Polarization Conversion	PCR (%)	Key Contribution
[43]	Aupattern /Polyimide/Au ground	$110\mu m$	$30\mu m$	2	Moderate	0.65–1.45	76	LP-LP	>80 %	First broadband THz polarization converter
[44]	Dual gold patches with planar chiral structure	$100\mu m$	$40\mu m$	2	Moderate	0.73–1.41	63.5	LP–LP	>95 %	Broadband transmission polarization conversion
[45]	Two metal gratings with metal stubs	$80\mu m$	$40\mu m$	3	High	0.75–1.0	28.6	LP–LP	>99 %	High transmission efficiency
[46]	Metal–dielectric–metal structure	$106\mu m$	$33\mu m$	2	Moderate	0.67–1.66	84.9	LP–LP	>88 %	Wide operating bandwidth
[47]	Gold metasurface on a dielectric substrate	$140\mu m$	$40\mu m$	1	low	0.75–1.13	40.4	LP–LP	>80 %	Broadband cross-polarization conversion
This Work	**Grating–Split Resonator Transmissive Metasurface**	**$100\mu m$**	**$30\mu m$**	**3**	**High**	**0.35-1.45**	**122.2**	**LP–LP Cross-Polarization**	**≈100**	**Compact geometry, optimized grating structure, CMA-based analysis, simple fabrication**

Conclusion

In this paper, a small three-layer transmissive terahertz metasurface for broadband linear cross-polarization conversion based on a grating-split resonator arrangement is presented. The proposed metasurface achieves a polarization conversion ratio close to unity (PCR $\leq$ 99%) over the entire 0.35-1.45 THz Operating range, corresponding to an extremely wide fractional bandwidth of 122.2%. The strong electromagnetic coupling between the asymmetric split-ring resonator and the

polarization-selective gratings enables broadband polarization conversion with efficient suppression of the co-polarized transmission. The transmission properties, surface current distributions, and Characteristic Mode Analysis (CMA) confirm the polarization conversion mechanism, with the broadband response primarily due to Modes 2–4, which are the dominant resonant modes. In addition, parametric optimization confirms that the modified geometric parameters provide high angular stability up to a 45° incidence angle. The proposed transmissive metasurface is well-suited for broadband terahertz systems that require efficient linear cross-polarization conversion across a wide frequency range. Wideband polarization conversion can alleviate polarization mismatch, improve link reliability across large spectral channels, and enable polarization diversity in terahertz wireless communication systems. The broadband operation provides high-resolution, multispectral imaging for terahertz sensing and imaging applications, with stable polarization over a broad frequency range. Furthermore, the high polarization conversion ratio and angular stability make the proposed metasurface a strong candidate for polarization manipulation in terahertz spectroscopy, imaging systems, and next-generation 6G communication platforms, where broadband, reliable polarization control is essential.

Conflict of Interest

The authors declare no known conflicts of interest that could influence the work described in this study.

Statement of Funding

No specific grant from a public, private, or nonprofit funding organization was obtained for this study.

Statement of Data Availability

Upon reasonable request, the corresponding author will provide the data that support the study's conclusions.

Statement of Ethics

Since there are no human subjects, human data, or human participants in this study, ethical approval was not needed.

Reference

1. Yang, Shing-Lung Steven, Ahmed A. Kishk, and Kai-Fong Lee. "Wideband circularly polarized antenna with L-shaped slot." *IEEE Transactions on Antennas and Propagation* 56.6 (2008): 1780-1783.
2. Falade, Oluyemi P., et al. "Single feed stacked patch circular polarized antenna for triple band GPS receivers." *IEEE Transactions on Antennas and Propagation* 60.10 (2012): 4479-4484.
3. Lin, Wei, and Hang Wong. "Wideband circular polarization reconfigurable antenna." *IEEE Transactions on Antennas and Propagation* 63.12 (2015): 5938-5944.
4. Ryzhkov, Alexander V., et al. "Calibration issues of dual-polarization radar measurements." *Journal of Atmospheric and Oceanic Technology* 22.8 (2005): 1138-1155.
5. Zhou Q G, Huang Z MandZhouW2021Infrared Technol. 43 817

6. Wang, Qingwang, et al. "Infrared image enhancement: A review." *IEEE Journal of Selected Topics in Applied Earth Observations and Remote Sensing* 18 (2024): 3281-3299.

7. Maltsev A, Perahia E, Maslennikov R, Sevastyanov A, and Khoryaev A 2010. IEEE Antenna. Wireless. PR. 9 413

8. Brand, G. F. "The strip grating as a circular polarizing beamsplitter." *International Journal of Infrared and Millimeter Waves* 23.9 (2002): 1271-1285.

9. Zhu, Weiren, et al. "Graphene-enabled tunability of optical fishnet metamaterial." *Applied Physics Letters* 102.12 (2013).

10. Zhao Y, Belkin M A, and Al`u A 2012 Nat. Commun. 3 8701

11. Shelby, Richard A., David R. Smith, and Seldon Schultz. "Experimental verification of a negative index of refraction." *Science* 292.5514 (2001): 77-79.

12. Wiltshire, M. C. K., et al. "Microstructured magnetic materials for RF flux guides in magnetic resonance imaging." *Science* 291.5505 (2001): 849-851.

13. Pendry, John B., et al. "Magnetism from conductors and enhanced nonlinear phenomena." *IEEE Transactions on Microwave Theory and Techniques* 47.11 (1999): 2075-2084.

14. Veselago, V. G. "The electrodynamics of substances with simultaneously negative values of and." *Usp. fiz. nauk* 92.3 (1967): 517-526.

15. Zhou, Qiangguo, et al. "High efficiency of broadband transmissive metasurface terahertz polarization converter." *Chinese Physics B* 32.2 (2023): 024201.

16. Sheheryar, Taha, et al. "An ultra-wideband terahertz linear cross-polarization converter with integrated biosensing for multi-disease diagnosis." *Journal of Materials Chemistry C* 13.24 (2025): 12460-12471.

17. Kang, Yongqiang, et al. "A broadband high-performance terahertz transmissive linear polarization converter using anisotropic metamaterials." *ACTA PHYSICA SINICA* 75.3 (2026).

18. Khalichi, Bahram, et al. "Split-Bridged Disk-Like Terahertz Metasurface: Enabling Ultra-Broadband Asymmetric Transmissive Co-to-Cross Polarization Conversion." *2025 International Applied Computational Electromagnetics Society Symposium (ACES)*. IEEE, 2025.

19. Parazzoli, C. G., et al. "Experimental verification and simulation of negative index of refraction using Snell's law." *Physical Review Letters* 90.10 (2003): 107401.

20. Yin, Xiaobo, et al. "Photonic spin Hall effect at metasurfaces." *Science* 339.6126 (2013): 1405-1407.

21. Mutlu, Mehmet, et al. "Diodelike asymmetric transmission of linearly polarized waves using magnetoelectric coupling and electromagnetic wave tunneling." *Physical Review Letters* 108.21 (2012): 213905.

22. Chen, Hou-Tong, et al. "Active terahertz metamaterial devices." *Nature* 444.7119 (2006): 597-600.

23. Xiao, Shuyuan, et al. "Active metamaterials and metadevices: a review." *Journal of Physics D: Applied Physics* 53.50 (2020): 503002.

24. Ye, Yuqian, and Sailing He. "90° polarization rotator using a bilayered chiral metamaterial with giant optical activity." *Applied Physics Letters* 96.20 (2010).

25. Song, Kun, et al. "Wide-angle 90°-polarization rotator using chiral metamaterial with negative refractive index." *Journal of Electromagnetic Waves and Applications* 26.14-15 (2012): 1967-1976.

26. Wang, Lei, et al. "Broadband tunable liquid crystal terahertz waveplates driven with porous

graphene electrodes." *Light: Science & Applications* 4.2 (2015): e253-e253.

27. Song, Kun, et al. "90° polarization rotator with rotation angle independent of substrate permittivity and incident angles using a composite chiral metamaterial." *Optics Express* 21.6 (2013): 7439-7446.

28. Song, Kun, et al. "A frequency-tunable 90-polarization rotation device using composite chiral metamaterials." *Applied Physics Letters* 103.10 (2013).

29. Tretyakov, Sergei, et al. "Waves and energy in chiral nihility." *Journal of electromagnetic waves and applications* 17.5 (2003): 695-706.

30. Kanda, N., K. Konishi, and M. Kuwata-Gonokami. "Terahertz wave polarization rotation with double-layered metal grating of complementary chiral patterns." *Optics Express* 15.18 (2007): 11117-11125.

31. Mutlu, Mehmet, et al. "Asymmetric chiral metamaterial circular polarizer based on four U-shaped split ring resonators." *Optics Letters* 36.9 (2011): 1653-1655.

32. C. Menzel, C. Rockstuhl, and F. Lederer, "Advanced Jones calculus for the classification of periodic metamaterials," Phys. Rev. A, vol. 82, no. 5, Art. no. 053811, Nov. 2010.

33. S. Wu, Z. Zhang, Y. Zhang, K. Zhang, L. Zhou, X. Zhang, and Y. Zhu, "Broadband wide-angle polarization converter based on a metasurface," Phys. Rev. Lett., vol. 110, no. 20, Art. no. 207401, May 2013.

34. J. B. Pendry, "A chiral route to negative refraction," Science, vol. 306, no. 5700, pp. 1353–1355, Nov. 2004.

35. J. Zhou, D. R. Chowdhury, R. Zhao, A. K. Azad, H. T. Chen, C. M. Soukoulis, A. J. Taylor, and J. F. O'Hara, "Terahertz chiral metamaterials with giant and dynamically tunable optical activity," Phys. Rev. B, vol. 86, no. 3, Art. no. 035448, Jul. 2012.

36. W. Chao, H. Li, Z. Wei, X. Yu, and C. T. Chan, "Illusion optics: The optical transformation of an object into another object," Phys. Rev. Lett., vol. 105, no. 24, Art. no. 247401, Dec. 2010.

37. X. Gao, X. Han, W. P. Cao, H. O. Li, H. F. Ma, and T. J. Cui, "Ultra-wideband and high-efficiency linear polarization converter based on transmissive metasurface," IEEE Trans. Antennas Propag., vol. 63, no. 1, pp. 352–362, Jan. 2015.

38. N. Liu, S. Kaiser, and H. Giessen, "Magnetoinductive and electroinductive coupling in plasmonic metamaterial molecules," Adv. Mater., vol. 20, no. 23, pp. 4521–4525, Dec. 2008.

39. Zhou, Xin, X. P. Zhao, and Yu Liu. "Disorder effects of left-handed metamaterials with unitary dendritic structure cell." *Optics Express* 16.11 (2008): 7674-7679.

40. Pozar, D. M. *Microwave Engineering*, 4th Edition, Wiley, 2012.

41. X. Gao *et al*., "A low-profile broadband circularly polarized patch antenna based on characteristic mode analysis," *IEEE Antennas Wireless Propag. Lett.*, vol. 20, pp. 214–218, 2021.

42. F. H. Lin and Z. N. Chen, "Low-profile wideband metasurface antennas using characteristic mode analysis," *IEEE Trans. Antennas Propag.*, vol. 65, no. 4, pp. 1706–1713, Apr. 2017.

43. Cheng, Yong Zhi, et al. "Ultrabroadband reflective polarization convertor for terahertz waves." *Applied Physics Letters* 105.18 (2014).

44. Xia, Rui, et al. "Broadband linear polarization conversion based on the coupling of bilayer metamaterials in the terahertz region." *Optics Communications* 383 (2017): 310-315.

45. Grady, Nathaniel K., et al. "Terahertz metamaterials for linear polarization conversion and anomalous refraction." *Science* 340.6138 (2013): 1304-1307.

46. Xia, Rui, et al. "Broadband terahertz half-wave plate based on anisotropic polarization conversion metamaterials." *Optical Materials Express* 7.3 (2017): 977-988.

47. Liu, Wenwei, et al. "Realization of broadband cross-polarization conversion in transmission mode in the terahertz region using a single-layer metasurface." *Optics Letters* 40.13 (2015): 3185-3188.